POTENTIAL CLINICAL SIGNIFICANCE

Nanomedicine: Nanotechnology, Biology, and Medicine
10 (2014) 1529–1538

nanomedicine
Nanotechnology, Biology, and Medicine

Original Article

nanomedjournal.com

A nano-disperse ferritin-core mimetic that efficiently corrects anemia without luminal iron redox activity

Jonathan J. Powell, PhD[a,*,1], Sylvaine F.A. Bruggraber, PhD[a,1], Nuno Faria, PhD[a], Lynsey K. Poots, BSc[a], Nicole Hondow, PhD[b], Timothy J. Pennycook, PhD[c,d], Gladys O. Latunde-Dada, PhD[e], Robert J. Simpson, PhD[e], Andy P. Brown, PhD[b,1], Dora I.A. Pereira, PhD[a,1]

[a]*MRC Human Nutrition Research, Elsie Widdowson Laboratory, Cambridge, UK*
[b]*Institute for Materials Research, School of Process, Environmental and Materials Engineering, University of Leeds, Leeds, UK*
[c]*SuperSTEM, Daresbury Laboratories, Warrington, UK*
[d]*Department of Materials, University of Oxford, Oxford, UK*
[e]*Diabetes & Nutritional Sciences Division, School of Medicine, King's College London, London, UK*

Received 10 September 2013; accepted 24 December 2013

Abstract

The 2-5 nm Fe(III) oxo-hydroxide core of ferritin is less ordered and readily bioavailable compared to its pure synthetic analogue, ferrihydrite. We report the facile synthesis of tartrate-modified, nano-disperse ferrihydrite of small primary particle size, but with enlarged or strained lattice structure (~2.7 Å for the main Bragg peak versus 2.6 Å for synthetic ferrihydrite). Analysis indicated that co-precipitation conditions can be achieved for tartrate inclusion into the developing ferrihydrite particles, retarding both growth and crystallization and favoring stabilization of the cross-linked polymeric structure. In murine models, gastrointestinal uptake was independent of luminal Fe(III) reduction to Fe(II) and, yet, absorption was equivalent to that of ferrous sulphate, efficiently correcting the induced anemia. This process may model dietary Fe(III) absorption and potentially provide a side effect-free form of cheap supplemental iron.

From the Clinical Editor: Small size tartrate-modified, nano-disperse ferrihydrite was used for efficient gastrointestinal delivery of soluble Fe(III) without the risk for free radical generation in murine models. This method may provide a potentially side effect-free form iron supplementation.

Key words: Iron oxide; Iron deficiency anemia; Oral iron; Ferrihydrite; Bioavailability

Despite all attempts to eradicate or even reduce iron deficiency anemia (IDA), it remains the most prevalent nutritional deficiency disorder in the world affecting around 1 billion people, of which nearly 400 million are children.[1] In childhood, IDA is associated with increased morbidity and reduced cognitive development and IDA remains on the World

Author Contributions: J.J.P. with input from S.F.A.B., D.I.A.P., N.F., R.J.S. and A.P.B. developed the hypothesis behind this research and designed the research; D.I.A.P., S.F.A.B, N.F., L.K.P., G.O.L-D and A.P.B. conducted the research; A.P.B. provided expertise and analysis on synthetic ferrihydrites; T.J.P provided technical expertise and analysis in SuperSTEM; D.I.A.P., A.P.B., N.H., R.J.S. and G.O.L-D analyzed data; D.I.A.P, A.P.B. and J.J.P. wrote the paper and had primary responsibility for final content. All authors read, input-to and approved the final manuscript.

Funding: This work was supported by the UK Medical Research Council (MRC) (U105960399) and MRC Technology Development Gap Fund (DGF). A.P. Brown is in receipt of an EPSRC Advanced Research Fellowship (EP/059678/1).

Statement of competing financial interests: The authors declare no conflict of interest but D.I.A.P., N.F., S.F.A.B. and J.J.P. wish to note that they are inventors on a patent detailing novel Fe(III) poly oxo-hydroxide structures, as described herein, and that may have further potential as commercial dietary supplements.

Abstracts presented: TEMA 14, China 2011; European Iron Club, Rennes 2012; Biological Barriers 2010, Saarland.

*Corresponding author.
E-mail address: jonathan.powell@mrc-hnr.cam.ac.uk (J.J. Powell).

[1]Indicates equal contribution.

http://dx.doi.org/10.1016/j.nano.2013.12.011
1549-9634/

Health Organisation (WHO) "top ten" hit list of targeted global health problems.[2-4]

Unlike most nutritional deficiencies, IDA is not confined to underdeveloped and developing countries: in the UK, for example, IDA affects around 5% of adults, nearly 12% of pre-school children and, in some areas, up to 25% of school children.[1,5,6]

To help combat IDA, oral iron supplementation needs to be well tolerated, cheap, safe and effective but current preparations fail in at least one of these criteria. Simple ferrous iron [Fe(II)] salts are most commonly used as these are inexpensive and the iron is well absorbed. However, they have lately come under the spotlight in high-profile intervention trials as they may enhance systemic infection rates, induce undesirable changes to commensal bacteria of the colon and increase pro-inflammatory signaling of the gut epithelium.[7-10] Some forms of ferric iron [Fe(III)] (e.g. ferric pyrophosphate) are considered safer and better tolerated in the gut lumen than Fe(II) but are poorly absorbed.[11-14] Chelation may overcome the issue of oral Fe(III) bioavailability but then marked enhancement of colon cancer risk is seen in rodent models using chelates of Fe(III) EDTA[15] or Fe(III) citrate[16] for example. In pursuit of strategies for optimal oral Fe supplementation we considered the chemical speciation of dietary Fe(III) and its processing in the gastrointestinal tract. In this respect, carefully designed studies have shown that Fe(III) is well absorbed from ferritin.[17-19] Ferritin is the broadly conserved biological storage form of iron and, thus, is found in both meat- and plant-based foods of the human diet: it is composed of a protein shell with a ferrihydrite-like mineral core.[20,21] Ferrihydrite is a poly oxo-hydroxide Fe(III) nanoparticle (about 2- to 5-nm diameter) with a precise atomic structure that still remains a matter of debate because its size and crystallographically defective nature make its definitive characterization challenging.[22-27] Notably, in ferritin, the surface of the ferrihydrite-like core appears destabilized (i.e. amorphous) compared to synthetic or geological ferrihydrite[20] which must be related to interactions between the ferritin protein shell and the ferrihydrite surface and may involve a phosphate-rich surface layer.[28] Indeed the morphology of the ferritin mineral core has been shown to follow the symmetry of the protein shell.[20,29] Such surface destabilization probably ensures that iron in ferritin is abnormally labile for an oxo-hydroxide in the presence of protons or ligands: thus it is rapidly turned over in the cell lysosome and will solubilize in gastric acid.[17,30-32] However, it is a matter of debate as to whether the protein shell and ferrihydrite-like core of ferritin control the slow release of Fe(III) ions from the gastric environment, or, if ferritin as a whole or as a protein-denuded mineral nanoparticle is rapidly emptied from the stomach and endocytosed by the intestinal epithelial cell and broken down intra-lysosomally.[18,32,33] Either way ferritin is an effective, bioavailable form of dietary iron that has, for example, led to considerable investment by the Global HarvestPlus Initiative in "bio-fortification" which involves the selection of staple food crops with enriched ferritin expression.[34-37]

Iron supplementation with pure ferritin would be immensely challenging due to the required scale of purification or the complexity of in vitro synthesis, and thus overall costs. However, synthetically, it may not be necessary to exactly mimic the ferritin molecule. When organic molecules are present during the pH-induced formation of aquated ferrihydrite they can do more than simply adsorb to the surface of freshly precipitated ferrihydrite. Ligands, such as low-molecular-weight organic acids, may abate the degree of iron–oxygen and hydroxyl octahedra linking, diminishing the primary particle size and retarding maturation and crystallization of the cross-linked polymer of freshly precipitated ferrihydrite.[38,39] We show here that simple aqueous conditions can be identified that allow small hydroxyl–carboxyl organic ligands to be co-precipitated with freshly forming ferrihydrite such that the ligand markedly disrupts ferrihydrite stability and, that in this fashion, bioavailable ferritin-core functional-mimetics were readily synthesised. For downstream applications (i.e. affordable supplementation) we focussed on cheap, generally recognized as safe (GRAS) dietary ligands to provide the modifications and we concentrated on nano-dispersion and enhanced rates of acid dissolution as initial desirable properties in light of current knowledge on dietary ferritin as an oral iron source.

Methods

Synthesis of solid ferrihydrite materials

The ligand-modified ferrihydrite materials were produced by co-precipitation and ligand substitution of oxo/hydroxy groups following the protocol described by Powell et al.[38] Briefly, an acidic concentrated stock solution of Fe(III) chloride was added to a solution containing the ligand, buffer and 0.9% (wt/vol) of electrolyte (sodium chloride; NaCl) or, in the case of synthetic ferrihydrite, simply 0.9% NaCl. The initial pH of the mixture was always below 2.0, and the iron was fully solubilized. The pH was then slowly increased by drop-wise addition of a concentrated solution of NaOH with constant agitation until reaching the desired final pH (ca. 7.4 for ligand-modified ferrihydrite and 7.4-8.2 for synthetic ferrihydrite). In the case of synthetic ferrihydrite the entire mixture was then oven dried at 45 °C for a minimum of 24 h. For the ligand-modified ferrihydrite materials, ultrafiltration (3,000 Da MWCO, Vivaspin®) followed by one H_2O_{UHP} wash was used to remove excess soluble ligand and buffer, i.e. non-bound or non-adsorbed to the nanoparticles (≥95% recovery according to the manufacturer's specifications), before the material was oven dried (again 45 °C) for at least 24 h.

Physicochemical characterization

Iron content and phase distribution

Total iron content was determined by inductively coupled plasma optical emission spectrometry (ICP-OES JY 2000, Horiba Jobin Yvon Ltd., Stanmore, UK). ICP-OES standards and samples were diluted in 5% HNO_3 to concentrations in the range 0-1000 ppm. Fractionation of the Fe into percentages of precipitated, nanoparticulate, and soluble Fe, for each of the Fe materials was achieved by centrifugation and ultrafiltration. Aqueous suspensions were centrifuged (10,000 × *g*, 5 min) and the sediment taken to be the precipitated fraction. In order to isolate the soluble Fe, and to distinguish it from disperse or colloidal (i.e. nanoparticulate) Fe, the supernatant was ultrafiltered (3,000 Da MWCO; 10,000 × *g*, 10 min). The Fe content

of all fractions (total, supernatant and ultrafiltrate) was determined by ICP-OES and expressed as percentage ± SD in relation to total Fe content as follows:

$$[(\%)\ \text{Fe precipitated}] = \left[\left(\text{Total Fe} - \text{Fe}_{\text{supernatant}}\right)/\text{Total Fe}\right] \times 100$$

$$[(\%)\ \text{Fe nanoparticulate}] = \left[\left(\text{Fe}_{\text{supernatant}} - \text{Fe}_{\text{ultrafiltrate}}\right)/\text{Total Fe}\right] \times 100$$

$$[(\%)\ \text{Fe soluble}] = [(\text{Fe}_{\text{ultrafiltrate}})/\text{Total Fe}] \times 100$$

The iron materials were further characterized in terms of particle morphology by high-angle annular dark-field aberration-corrected scanning transmission electron microscopy (HAADF-STEM), X-ray diffraction, Fourier transform infrared spectroscopy (FTIR), electron energy-loss spectroscopy (EELS) and acid dissolution profiles. These methods are detailed in Supplementary Materials.

Animal studies

Six-week-old male mice, CD1 strain (Charles Rivers, Kent, UK), were used for the "ferrozine" study. Mice were housed in a light- and temperature-controlled room with ad libitum access to standard pellet diet and water. Animal care and the regulation of scientific procedures met the criteria laid down by the United Kingdom Animals (Scientific Procedures) Act 1986. Iron deficiency was induced by feeding 3- to 4-week-old mice a purified low-iron diet (Harlan Teklad, USA) with less than 1 mg Fe/kg for at least 2 weeks. Iron absorption studies were performed on iron-deficient mice fasted for ca. 16 h prior to the oral Fe dose. The Fe materials were prepared as described above at 20 mM Fe, labeled with ^{59}Fe (ca. 3.1 MBq) at the time of synthesis (intrinsic labeling), and administered by oral gavage directly into the stomach as a single 100-μl dosage. Two oral doses of 10 mM ferrozine[40] or water (control) were given 1 h prior to and during the gavage with the Fe compounds. Mice were left for 4 h with free access to drinking water until sacrifice and tissue collection. The stomach, small intestine and cecum plus colon were removed. The duodenum was removed and rinsed with 0.15 M NaCl. Intestinal tissue samples and duodenal washings were counted for ^{59}Fe using a LKB Wallac gamma counter. The carcass was counted for ^{59}Fe in a small animal whole body gamma counter (LIVE-1, Technical Associates, Canoga Park, CA). Standards were also measured in both counters to correct for the difference in sensitivity. Mucosal transfer was the amount of ^{59}Fe in the carcass expressed as a percentage of administered dose: i.e. the amount of ^{59}Fe radioactivity in the carcass 4 h after the gavage and is expressed as percentage of the total amount of radioactivity that is emptied out of the stomach. The soluble ferric iron control was Fe(III) nitrilotriacetate complex (i.e. Fe(III) NTA).

The bioavailability study in rats was conducted by MPI Research (Michigan, USA) and was approved by the Institutional Animal Care and Use Committee (IACUC) (MPI study protocol number 1925-001) following United States Animal Welfare Regulations. Hemoglobin was measured by clinical pathology as part of a complete blood count (CBC) panel. The increase in hemoglobin at day 14 was used as a measure of the bioavailability of the ligand-modified ferrihydrite in comparison with synthetic ferrihydrite and the current gold standard for iron supplementation (Fe(II) sulphate). Male Sprague–Dawley [Crl:CD® (SD)] rats (n = 32) were approximately 21 days old at arrival (Charles River Laboratories). The animals were housed individually in polyboxes with toys and fed Block Lab Diet® Certified Rodent Diet #5002 (PMI Nutrition International, Inc), ad libitum during the acclimation period (not less than 7 days). The control diet, i.e. the iron-deficient (ID) diet (AIN-93G Purified Rodent Diet, Dyets Inc., PA, USA) was administered to all animals from day 0 to day 24 (for the complete diet composition see Supplementary Table 2). The incorporation of the iron materials into the diets (~30 mg Fe/kg$_{\text{diet}}$) and pelletization through extrusion were carried out by Dyets Inc. Other than the varying Fe compound, the diets were equivalent and conformed to AIN-93G-purified rodent diet.[41]

Administration of the test diets, ID diet fortified with Fe(II) sulphate, ID diet fortified with synthetic ferrihydrite, and ID diet fortified with tartrate-modified ferrihydrite, began on day 25. Three groups of eight male rats each were administered the test diets. One additional group of eight animals served as the no-iron control and continued to receive the un-supplemented ID diet. The test and control diets were administered for 14 days (i.e. until day 38). Rats consumed tap water and the control or test diets ad libitum throughout the study. Body weights were measured and recorded weekly. Blood samples for clinical chemistry evaluations were collected on days −1, 25, and 39. After the study termination (day 39) the rats were anaesthetized by CO_2 inhalation and animals were euthanized by exsanguination.

Results

Iron material characterization

With initial screening in vitro we sought common GRAS (or "biologically safe") ligands that would enable the formation of nano-dispersed, rather than aggregated or agglomerated, ferrihydrite materials upon titration of an acidic Fe(III)/ligand solution with base.

To ensure repeatability we used two separate buffers in parallel, namely adipate and tryptophan. Consistently, 40 mM Fe(III) and sub-equimolar tartrate yielded nano-dispersed Fe oxo-hydroxide materials: for optimal yield of the nano-disperse material the Fe(III)/tartrate ratio was 2:1 and pH buffered to greater than 7.0 (≥90% yield: open triangles, Figure 1, *A* and Supplementary Figure S1A). Buffer alone (adipate or tryptophan) had no effect and Fe(III) oxo-hydroxide aggregation and precipitation preceded as normal (closed circles, Figure 1, *A* and Supplementary Figure S1A). We aimed to obtain dry materials that would re-disperse once aquated at the appropriate pH so, we next confirmed that, when re-introduced into the original volume of aqueous solution, the material again was nano-dispersed or precipitated according to pH in line with the original titration profile

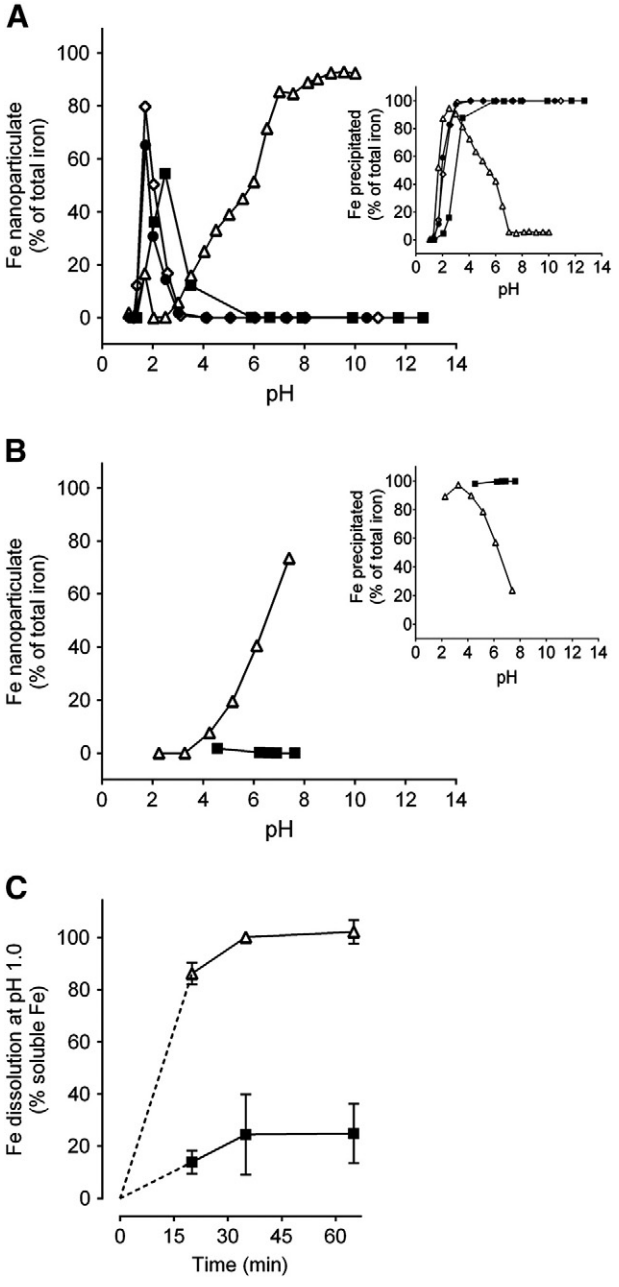

Figure 1. Formation of tartrate-modified ferrihydrite in adipate buffer as a function of pH. **(A)** Dispersed or colloidal (i.e. nanoparticulate) iron, determined following centrifugation and ultrafiltration to remove soluble iron (main panel), and precipitated (i.e. agglomerated) iron, determined following centrifugation (inset). Closed squares show synthetic ferrihydrite precipitated from an Fe(III) chloride solution; open triangles show modified ferrihydrite precipitated from an Fe(III) chloride solution in the presence of sodium tartrate and adipate buffer (Fe/tartrate/adipate = 1:0.5:0.5); closed circles and open diamonds show ferrihydrite precipitated from an Fe(III) chloride solution in the presence of adipate alone (Fe/adipate = 1:0.5 and 1:1 respectively). **(B)** Percentage of nanoparticulate iron (main panel) and precipitated iron (inset) for the synthetic (closed squares) and tartrate-modified (open triangles) ferrihydrite materials (molar ratios as above) re-suspended in the original volume of aqueous solution. **(A** and **B)** All values are expressed as a percentage of total iron in the initial solution as described in Methods. **(C)** Simulated gastric dissolution at pH 1.0 of dried synthetic ferrihydrite (closed squares) and tartrate-modified ferrihydrite that had been precipitated in the presence of tartrate and adipate (open triangles), at molar ratios as above, and then dried. Data were obtained following 5-min ultrafiltration (3000 Da MWCO); data are mean ± SD, $n = 3$.

(open triangles, Figure 1, *B* and Supplementary Figure S1B). To determine whether acid-driven dissolution was enhanced with tartrate modification we followed iron solubility in HCl at pH 1, as recently undertaken by Hilty et al.[42] as a proxy for Fe(III) bioavailability following oral dosing. The tartrate-modified ferrihydrite showed markedly greater solubility than similarly prepared ferrihydrite precipitated in the absence of tartrate (Figure 1, *C* and Supplementary Figure S1C).

To determine whether nano-dispersion alone or modification of the ferrihydrite primary particles (i.e. modification of synthetic ferrihydrite) had occurred during co-precipitation with tartrate, we used powder X-ray diffraction (XRD), analytical electron microscopy and Fourier transform infrared spectroscopy (FTIR). Initial identification of synthetic ferrihydrite (i.e. the dried control material without ligand modification) was performed using powder XRD (Figure 2): Two broad peaks were present, centered at ~35° and 62° 2θ (2.6 Å and 1.5 Å respectively), and are characteristic of two-line ferrihydrite.[43] Spherical aberration-corrected high-angle annular dark-field (HAADF) scanning transmission electron microscopy (STEM) imaging (Figure 2) indicated that the average crystallite sizes ranged from 2 to 4 nm. This size, and the morphology, were exactly as expected for two-line ferrihydrite.[24] Contrast in HAADF-STEM images is sensitive to atomic number (to the power of about 1.7) and spherical aberration correction enables atomic contrast to be obtained.[20] Thus the image of synthetic ferrihydrite (Figure 2, *D*) emphasizes the lattice positions of the iron atoms in this nanocrystalline material (since iron is the heaviest element in ferrihydrite).

Synthesis, as above, in the presence of tartrate (Fe/tartrate = 2:1), followed by ultrafiltration (3 kDa MWCO), washing and drying, yielded a powder XRD pattern with broader, less well-defined Bragg peaks, shifted to 33° and 61° 2θ respectively (2.7 Å and 1.5 Å; Figure 2). Consistent with the qualitative changes in broadening of the XRD pattern, corresponding HAADF-STEM images highlighted the notable nanoparticle dispersion and a marked decrease in overall crystallite order and size (to ca. 1-1.5 nm) of the tartrate-modified ferrihydrite (Figure 2, *A* and *B*) compared to synthetic ferrihydrite (Figure 2, *D*).

The infrared spectrum of synthetic ferrihydrite (black line, Figure 3) was entirely consistent with that previously reported,[44,45] whereas that of ferrihydrite precipitated in the presence of tartrate (Fe/tartrate = 2:1), and then ultrafiltered, washed and dried (red line, Figure 3), showed a mixed profile of tartrate (green line, Figure 3) plus ferrihydrite (black line, Figure 3) but with no evidence of buffer (tryptophan) which, if present, would show strong unique peaks at ~700 and 3350 cm^{-1} (blue line, Figure 3): moreover, the tartrate-modified ferrihydrite (red line, Figure 3) generated only broad tartrate peaks, distinct to those of sodium tartrate (e.g. the sharp doublet of ~1100 cm^{-1}; green line, Figure 3). The similarity between the infrared spectra for tartrate and adipate (particularly at ~3000 cm^{-1}) precludes such discriminatory comparisons when using the adipate buffer for synthesis.

Transmission electron microscopy (TEM) with electron energy-loss spectroscopy (EELS) was used to probe the local iron environments of the ferrihydrite materials (Figure 4). The Fe

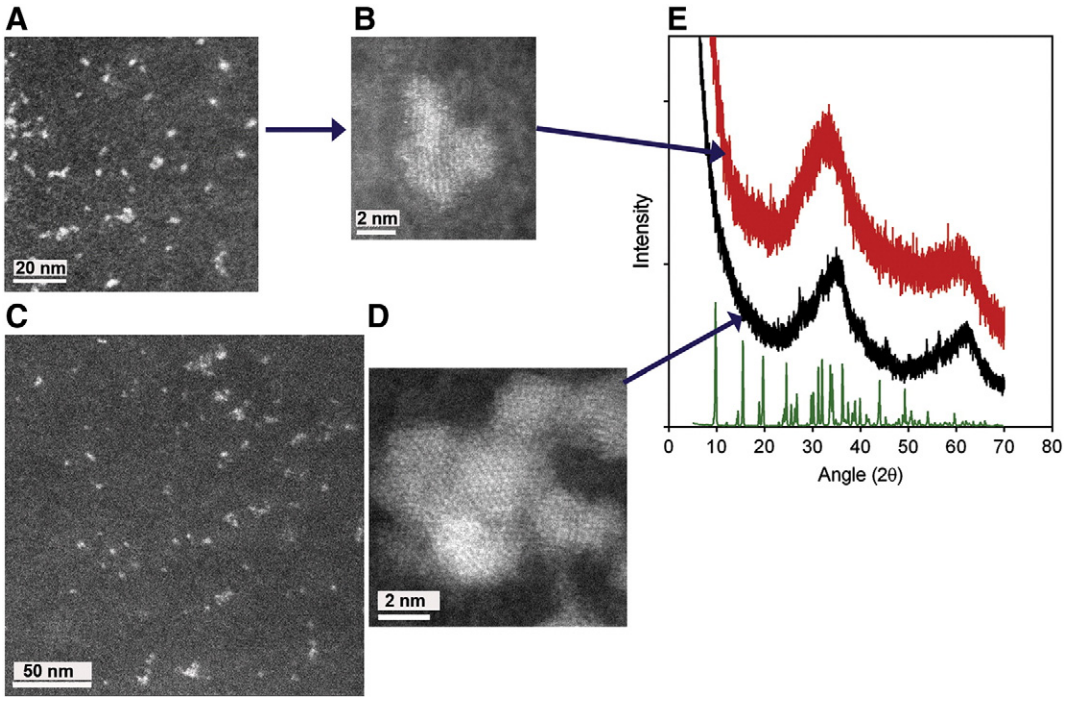

Figure 2. Structural characterization of the ferrihydrite. **(A-D)**, High-angle annular dark-field, aberration-corrected, scanning transmission electron microscopy (HAADF-STEM) images of tartrate-modified ferrihydrite in tryptophan **(A, B)** or adipate buffer **(C)**, and of synthetic (unmodified) ferrihydrite **(D)**. Scale bars are 50 nm **(A** and **C)** or 2 nm **(B** and **D)**. **(E)** X-ray diffraction patterns of synthetic ferrihydrite (black) and tartrate-modified ferrihydrite (red). Both patterns have peaks characteristic of ferrihydrite, with the synthetic ferrihydrite peaks centred at 35° and 62° 2θ (2.6 Å and 1.5 Å, respectively) and the tartrate-modified ferrihydrite peaks centered at 33° and 61° 2θ (2.7 Å and 1.5 Å, respectively), indicating expansion of the ferrihydrite lattice. Sodium tartrate is shown in green. Synthetic ferrihydrite was precipitated from an Fe(III) chloride solution and tartrate-modified ferrihydrite from an Fe(III) chloride solution in the presence of tartrate and tryptophan buffer (Fe/tartrate/tryptophan = 1:0.5:0.375). Excess ligand and buffer were removed from the modified material by ultrafiltration and washing prior to drying as described in Methods.

$L_{2,3}$-edge spectrum of the synthetic (unmodified) material was again consistent with that of synthetic ferrihydrite[27,46,47] while the tartrate-modified ferrihydrite Fe spectrum was almost identical suggesting that the ferrihydrite (or at least the Fe(III)) nature of the material was retained (Figure 4). An apparent very minor shift of the Fe L_3-peak maxima from 709.5 eV (Fe(III)) toward 707.5 eV (Fe(II)) should be viewed with caution as our previous data have shown that even with carefully controlled electron exposure, organic moieties will enhance the susceptibility of ferrihydrite to irradiation damage.[27,46,47] The same should be noted for the carbon and oxygen *K*-edges at around 285 and 530 eV respectively, although the modified material shows, as expected, a much greater content of the organic-derived signals (Figure 4).

Taken together the XRD, STEM, FTIR and EELS data show that the tartrate-modified ferrihydrite is a disrupted or strained ferrihydrite structure where the tartrate ligand has been incorporated into the particles during co-precipitation and we suggest that this leads to a more acid-labile structure. Certainly, the core ferrihydrite is smaller and less crystalline and has larger lattice spacings in the tartrate-modified material (Figures 2 and 4). Additionally, our data are also consistent with ligand bonding, between the tartrate, with its moderate affinity for iron (log $K_{\text{eff}} = 6.49$ at pH 3.54, 20 °C),[48,49] and the surface of the ferrihydrite nanoparticles, so inhibiting further crystallization and growth[39] and allowing nano-dispersion in aquated systems (Figure 1).

Bioavailability

Therapeutic supplementation with oral Fe(II) salts (e.g. ferrous sulphate) induces significant gastrointestinal side effects in ~30% of subjects affecting compliance and thus effectiveness.[50,51] This issue is considered, mostly to relate to iron redox cycling in the gut lumen leading to the generation of reactive oxygen species.[52] Iron (III) salts are less prone to the initiation of redox cycling in this environment but are insoluble at intestinal pH and thus are poorly absorbed.[53] Iron (III) chelates overcome the solubility issue but are expensive compared to salts and still undergo reduction at the mucosal surface, probably via duodenal cytochrome B.[54] Here we show that when given by oral gavage to mice, tartrate-modified ferrihydrite is absorbed as efficiently as the Fe(III) chelate, ferric nitrilotriacetate (Fe(III)NTA) (Figure 5, *A*). However, when the lumen of the gut was first flooded with ferrozine, an Fe(II) chelator that traps the luminal/mucosal surface-reduced iron,[40] there was no impact on absorption of the tartrate-modified ferrihydrite, whereas Fe(III)NTA absorption was almost completely inhibited, confirming Fe(III)NTA requirement for reduction prior to uptake, and in contrary to that of the modified ferrihydrite (Figure 5, *A*).

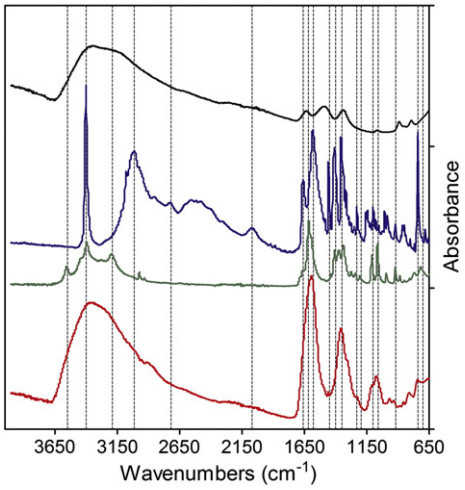

Figure 3. Fourier transform infrared (FTIR) spectroscopy of the ferrihydrite. Synthetic (unmodified) ferrihydrite is shown in black, tryptophan in blue, sodium tartrate in green and the tartrate-modified ferrihydrite is in red. Unique tartrate but no tryptophan signatures are revealed in the modified material. Synthetic and tartrate-modified ferrihydrite were prepared as per Figure 2.

Finally, in iron-deficient anemic rats, tartrate-modified ferrihydrite, added to a standard diet at 30 mg Fe/kg_{diet}, was able to restore hemoglobin levels over 2 weeks, in line with that of the gold standard ferrous sulphate (Figure 5, *B*). Synthetic ferrihydrite, added to the diet, had no impact on hemoglobin levels added to the same diet, at the same dose (Figure 5, *B*). There was no significant difference in the body weights of the animals on the tartrate-modified ferrihydrite supplemented diet in comparison with those on the diet supplemented with ferrous sulphate (Supplementary Table S1).

Discussion

Co-precipitation of metal ion hydroxides and organic moieties to form metal oxo-hydroxides with a degree of modification is well established. Typically this involves organic adsorption onto the freshly formed oxo-hydroxide nanoparticles which, for small anions or ligands, may enhance the formation of a meta-stable, crystalline phase.[55] For large molecules, such as polymeric sugars, the surface coat acts to prevent secondary agglomeration and aggregation, a property that has found beneficial use in the production of both intravenous and oral therapeutic iron preparations.[56-60] Overall, however, in such studies the primary particle (crystallite) of the metal oxo-hydroxide appears pure in its internal structure. In contrast, here we demonstrate that the polymeric, evolving primary particle of ferrihydrite, can be rendered impure or "doped" with a low-molecular-weight organic acid under specific conditions of co-precipitation. For tartrate the spacing between carboxyl and OH pairs that Fe ions might bind to during complexation in solution is similar to the distance between Fe atoms in partially ordered ferrihydrite.[39] This might enable the organic acid to become trapped in, as well as adsorbed on, precipitating ferrihydrite particles. Certainly, if hydrolysis proceeds too rapidly the organic acid ligand fails to be incorporated within the evolving ferrihydrite particles and, instead, is simply adsorbed onto the primary particles. At the other extreme, excessive concentration of ligand may inhibit sufficient hydrolysis of iron. However, at appropriate ratios of Fe/ligand/OH^-, ligand-modified ferrihydrite can be achieved, the properties of which differ substantially to the pure synthetic oxo-hydroxides due to marked changes in crystallinity, surface charge and stability.

Our data are consistent with the recent studies of Eusterhues et al.[61] who demonstrated that organic ligands may indeed modify, through inclusion, and disruption of iron octahedral cross-linking, the inter-atomic bond distances (*d*-spacings) and particle size of ferrihydrite. More recently, Mikutta[62] has shown, with similar iron/ligand co-precipitation studies, that hydroxyl-benzoic acids may trigger the formation of small ferrihydrite nanoparticles with increased structural strain, but without altered *d*-spacing, in equilibrium with a fraction of lower-molecular-weight Fe(III) hydroxybenzoate complexes. In our system, however, the ligand-induced strain is sufficient to alter *d*-spacing (Figure 2). Furthermore, infrared analysis of ultrafiltered and washed material, obtained following repeated centrifugation steps, demonstrates co-association of ferrihydrite and bound tartrate but not buffer, again consistent with inclusion of tartrate in the ferrihydrite particles (Figure 3). Taken together our studies indicate that the active material reported herein is a ligand-modified form of ferrihydrite and not simply a mixture of small ferrihydrite particles and low-molecular-weight iron complexes. Indeed, dissolution studies indicate that all of the iron, and not just a labile fraction, is rendered soluble under lysosomal conditions (Figure 1, *C*). Secondly, ferrozine fails, *entirely*, to block intestinal uptake of the iron from tartrate-modified ferrihydrite (Figure 5, *A*). This again confirms that there is no labile Fe(III) fraction associated with the tartrate-modified ferrihydrite. Ferrozine is an Fe(II) chelator that has been well shown, both in vivo and in vitro, to markedly inhibit iron absorption from soluble Fe(III) complexes because these have an absolute requirement for reduction prior to absorption.[40,63-66] Ferrozine traps the reduced iron (i.e. Fe(II)) and prevents iron absorption but no such effect was seen here with tartrate-modified ferrihydrite. Thirdly, our recent cellular studies with electron microscopy and inhibition of cellular endocytosis, demonstrate significant intestinal cell uptake of whole nanoparticles.[67]

The aims of this work were not to mimic the ferrihydrite-like core of ferritin in appearance or molecular detail but, rather, in terms of its functional properties that allow for iron bioavailability following ingestion by humans: namely, nanoparticle dispersion and an enhanced rate of acid-induced dissolution (and, presumably, chelator-induced dissolution). Phosphate, for example, which is clearly involved in interactions between the ferritin protein and its ferrihydrite-like core, probably contributes to core instability[28,68] and can certainly alter the structure of ferrihydrite following co-precipitation and hydrothermal annealing.[69] However, in our work, additional phosphate ions provided no further effect over tartrate alone in destabilizing synthetic ferrihydrite and, when used instead of organic acid ligand, phosphate was ineffective (data not shown). The

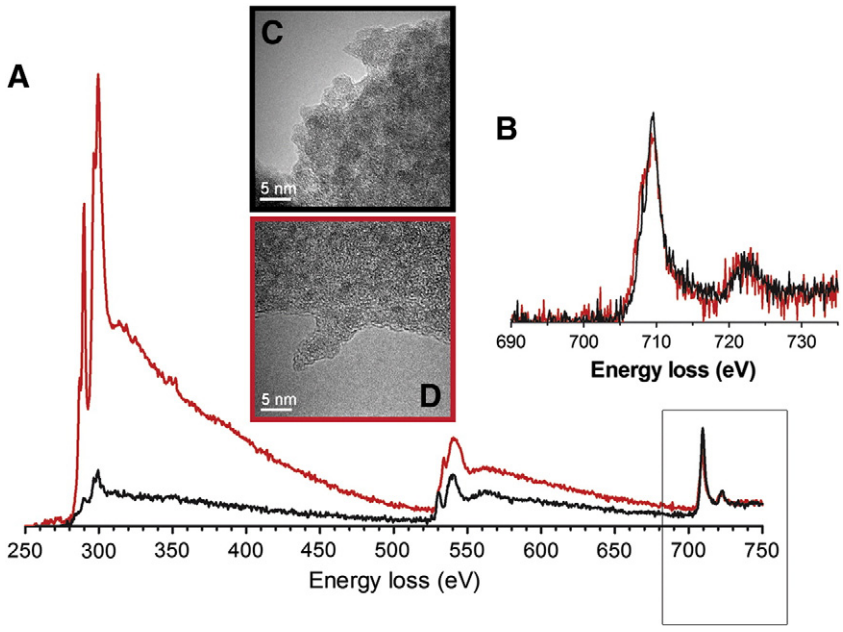

Figure 4. Electron microscopy-based characterization of tartrate-modified ferrihydrite (red) against synthetic ferrihydrite (black). **(A)** Background-stripped electron energy-loss spectra (EELS) for the combined C *K*-edges (285 eV), Ca $L_{2,3}$-edges (346 eV), O *K*-edges (530 eV) and Fe $L_{2,3}$-edges (709.5 eV) normalized to the continuum intensity post the Fe $L_{2,3}$-edges. **(B)** individual background-stripped Fe $L_{2,3}$-edges. The unaltered shape of the Fe $L_{2,3}$-edges indicates that the Fe−$(O, OH)_6$ octahedra remain relatively unchanged after tartrate modification: i.e. the material remains Fe(III). **(C** and **D)** Bright-field transmission electron microscopy (TEM) images of synthetic ferrihydrite **(C)** and tartrate-modified ferrihydrite **(D)** agglomerates suspended over holes in the TEM support film (see supplementary methods for details of specimen preparation). Diffraction contrast from individual crystallites produces dark regions in the images, the size of which confirms the reduced crystallite size of the modified material. Synthetic ferrihydrite was precipitated from an Fe(III) chloride solution and tartrate-modified ferrihydrite from an Fe(III) chloride solution in the presence of tartrate and adipate buffer (Fe/tartrate/adipate = 1:0.5:0.5).

additional factor of the protein shell in ferritin, as opposed to the protein-free structures reported herein, may explain differing phosphate sensitivities. In fact, the ligand-destabilized synthetic ferrihydrite of this report may even better mimic dietary Fe(III) that is dissolved under acidic, gastric conditions but then re-precipitates under the much less acidic intestinal conditions: endogenous ligands abound in the gastrointestinal lumen and soluble mucin (once referred to as gastroferrin)[70] maintains the ferrihydrite nano-disperse.[71] It is noteworthy that, systemically, the lysosome is used almost exclusively as *the* safe environment for macromolecular iron turnover (e.g. cycling and re-cycling of hemoglobin, Fe transferrin and ferritin) so it is not inconceivable that nanoparticulate iron is also acquired by the gut through intestinal endocytosis and then dissolved by lysosomal acid and ligands.[31,72]

In the pursuit of novel, safe iron fortificants, Hilty et al.[73] also demonstrated that nano sized Fe(III)-based particles are more bioavailable than bulk forms and are handled safely by the gut without contributing to abnormal tissue loading, although these authors regarded slow-release, gastric acid dissolution as an explanation for bioavailability of their Fe(III) nanomaterials. Whether dissolved in the gastric acid environment or the intestinal enterocyte lysosome, we concur with Hilty et al.[73] that labile forms of nanosized Fe(III) would join the common (dietary) iron pool before basolateral export from the enterocyte, ensuring normal homeostatic control of these forms of iron. Moreover, for these nanomaterials the residual unabsorbed Fe(III) should transit the remaining gastrointestinal tract in a relatively safe, non-redox active form whether it be as the original nanostructure or re-precipitated following gastric emptying. Unlike previously reported nano Fe(III) materials, produced by flame pyrolysis[42,73] and with organoleptic properties suitable for *fortification*[a], our approach focuses on cheap, GRAS reagents and facile synthesis to enable inexpensive but safe and effective *supplementation*[a] which, as the World Health Organisation has noted, is especially required in developing and underdeveloped countries.[1]

Overall, the ligand-modified ferrihydrite materials reported herein are noteworthy for their very small primary particle size (<5 nm) and enlarged lattice (circa 2.7 Å for the main Bragg peak) compared to synthetic ferrihydrite (2.6 Å). These findings therefore suggest that with appropriate buffers and Fe(III)/ligand/OH^- ratios, conditions can be achieved for ligand inclusion into the developing ferrihydrite particles, retarding both growth and crystallization, and favoring stabilization of the cross-linked polymeric structure. Such materials could have beneficial application in one key global health priority, namely the prevention and treatment of iron deficiency anemia without side effect-inducing redox cycling in the gastrointestinal tract.

[a] Iron fortificants are added to foods whereas iron supplements are taken as oral tablets or capsules and typically at higher iron doses than for fortificants. The materials reported herein are suitable as supplements due to cheap manufacturing costs but lack the organoleptic properties (typically are too dark in color) for fortificants.

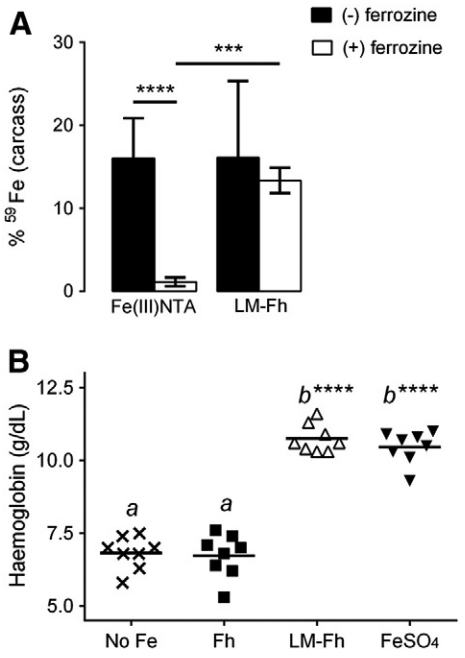

Figure 5. Comparative iron absorption and bioavailability of ligand-modified ferrihydrite. **(A)** Effect of ferrozine on the absorption of soluble ferric iron (i.e. Fe(III) NTA) and nanoparticulate, tartrate-modified ferrihydrite (i.e. LM-Fh) in male CD1 mice. Mice were orally gavaged with ^{59}Fe-labeled compounds with (open bars) or without (closed bars) ferrozine treatment as detailed in Methods. Values are mean ± SD, $n = 7$ per group. ***$P = 0.0009$; ****$P < 0.0001$; other comparisons are not significantly different. **(B)** Hemoglobin levels of anemic Sprague–Dawley male rats following 2-week treatment with diets fortified with the different iron compounds: No Fe = control diet with no supplemental iron (3.1 ± 0.6 mg Fe/kg$_{diet}$); Fh = synthetic ferrihydrite (35.7 ± 0.1 mg Fe/kg$_{diet}$); LM-Fh = tartrate-modified ferrihydrite (31.4 ± 0.5 mg Fe/kg$_{diet}$); $FeSO_4$ = Fe(II) sulphate (35.8 ± 0.1 mg Fe/kg$_{diet}$). Tartrate-modified ferrihydrite was precipitated from an Fe(III) chloride solution in the presence of tartrate and adipate buffer (Fe/tartrate/adipate = 1:0.5:0.5). Means with a common letter are not statistically different from one another, and means labeled with **** are statistically different from the control diet (No Fe), $P < 0.0001$, $n = 8$ per group.

Acknowledgments

This is a publication of the UK Medical Research Council (MRC). We are grateful to the EPSRC for access to the UK national facility for aberration-corrected STEM (SuperSTEM) and Andrew Bleloch for providing the HAADF-STEM images of synthetic ferrihydrite.

Appendix A. Supplementary data

Supplementary data to this article can be found online at http://dx.doi.org/10.1016/j.nano.2013.12.011.

References

1. De Benoist B, McLean E, Egli I, Cogswell M. *Worldwide prevalence of anaemia 1993-2005*. Geneva, Switzerland: World Health Organization; 2008.
2. Ezzati M, Lopez AD, Rodgers A, Vander Hoorn S, Murray CJ. Selected major risk factors and global and regional burden of disease. *Lancet* 2002;**360**(9343):1347-60.
3. WHO. The World Health Report. Reducing risks, promoting healthy life. Geneva, Switzerland: World Health Organization; 2002.
4. Stoltzfus RJ. Iron deficiency: global prevalence and consequences. *Food Nutr Bull* 2003 Dec;**24**(4 Suppl):S99-S103.
5. Adamson EA, Bailey GR, Richards N, Wilson H. Prevalence of anaemia in an inner city primary school population. *Arch Dis Child* 2008;**93**(5):453.
6. Barroso F, Allard S, Kahan BC, Connolly C, Smethurst H, Choo L, et al. Prevalence of maternal anaemia and its predictors: a multi-centre study. *Eur J Obstet Gynecol Reprod Biol* 2011 Nov;**159**(1):99-105.
7. Sazawal S, Black RE, Ramsan M, Chwaya HM, Stoltzfus RJ, Dutta A, et al. Effects of routine prophylactic supplementation with iron and folic acid on admission to hospital and mortality in preschool children in a high malaria transmission setting: community-based, randomised, placebo-controlled trial. *Lancet* 2006;**367**(9505):133-43.
8. Dostal A, Chassard C, Hilty FM, Zimmermann MB, Jaeggi T, Rossi S, et al. Iron depletion and repletion with ferrous sulfate or electrolytic iron modifies the composition and metabolic activity of the gut microbiota in rats. *J Nutr* 2012;**142**(2):271-7.
9. Werner T, Wagner SJ, Martinez I, Walter J, Chang JS, Clavel T, et al. Depletion of luminal iron alters the gut microbiota and prevents Crohn's disease-like ileitis. *Gut* 2011;**60**(3):325-33.
10. Carrier J, Aghdassi E, Cullen J, Allard JP. Iron supplementation increases disease activity and vitamin E ameliorates the effect in rats with dextran sulfate sodium-induced colitis. *J Nutr* 2002;**132**(10):3146-50.
11. Navas-Carretero S, Sarria B, Perez-Granados AM, Schoppen S, Izquierdo-Pulido M, Vaquero MP. A comparative study of iron bioavailability from cocoa supplemented with ferric pyrophosphate or ferrous fumarate in rats. *Ann Nutr Metab* 2007;**51**(3):204-7.
12. Moretti D, Zimmermann MB, Wegmuller R, Walczyk T, Zeder C, Hurrell RF. Iron status and food matrix strongly affect the relative bioavailability of ferric pyrophosphate in humans. *Am J Clin Nutr* 2006;**83**(3):632-8.
13. Davidsson L, Kastenmayer P, Szajewska H, Hurrell RF, Barclay D. Iron bioavailability in infants from an infant cereal fortified with ferric pyrophosphate or ferrous fumarate. *Am J Clin Nutr* 2000;**71**(6):1597-602.
14. Zimmermann MB, Biebinger R, Egli I, Zeder C, Hurrell RF. Iron deficiency up-regulates iron absorption from ferrous sulphate but not ferric pyrophosphate and consequently food fortification with ferrous sulphate has relatively greater efficacy in iron-deficient individuals. *Br J Nutr* 2011;**105**(8):1245-50.
15. Seril DN, Liao J, Ho KL, Warsi A, Yang CS, Yang GY. Dietary iron supplementation enhances DSS-induced colitis and associated colorectal carcinoma development in mice. *Dig Dis Sci* 2002;**47**(6):1266-78.
16. Radulescu S, Brookes MJ, Salgueiro P, Ridgway RA, McGhee E, Anderson K, et al. Luminal iron levels govern intestinal tumorigenesis after apc loss in vivo. *Cell Rep* 2012;**2**(2):270-82.
17. Jin F, Frohman C, Thannhauser TW, Welch RM, Glahn RP. Effects of ascorbic acid, phytic acid and tannic acid on iron bioavailability from reconstituted ferritin measured by an in vitro digestion-Caco-2 cell model. *Br J Nutr* 2009;**101**(7):972-81.
18. Lonnerdal B, Bryant A, Liu X, Theil EC. Iron absorption from soybean ferritin in nonanemic women. *Am J Clin Nutr* 2006;**83**(1):103-7.
19. Zhang L, Fischer W, Pippel E, Hause G, Brandsch M, Knez M. Receptor-mediated cellular uptake of nanoparticles: a switchable delivery system. *Small (Weinheim an der Bergstrasse, Germany)* 2011;**7**(11):1538-41.
20. Pan YH, Sader K, Powell JJ, Bleloch A, Gass M, Trinick J, et al. 3D morphology of the human hepatic ferritin mineral core: new evidence for a subunit structure revealed by single particle analysis of HAADF-STEM images. *J Struct Biol* 2009;**166**(1):22-31.

21. Wang Z, Li C, Ellenburg M, Soistman E, Ruble J, Wright B, et al. Structure of human ferritin L chain. *Acta Crystallogr* 2006;**62**(Pt 7): 800-6.
22. Barron V, Torrent J, Michel FM. Critical evaluation of the revised akdalaite model for ferrihydrite—discussion. *Am Mineral* 2012;**97**(1): 253-4.
23. Drits VA, Sakharov BA, Salyn AL, Manceau A. Structural model for ferrihydrite. *Clay Miner* 1993;**28**(2):185-207.
24. Janney DE, Cowley JM, Buseck PR. Transmission electron microscopy of synthetic 2-and 6-line ferrihydrite. *Clay Clay Miner* 2000;**48**(1): 111-9.
25. Michel FM, Ehm L, Antao SM, Lee PL, Chupas PJ, Liu G, et al. The structure of ferrihydrite, a nanocrystalline material. *Science* 2007;**316** (5832):1726-9.
26. Paktunc D, Manceau A, Dutrizac J. Incorporation of Ge in ferrihydrite: implications for the structure of ferrihydrite. *American Mineralogist* 2013;**98**(5–6):848-58.
27. Pan YH, Vaughan G, Brydson R, Bleloch A, Gass M, Sader K, et al. Electron-beam-induced reduction of Fe(3+) in iron phosphate dihydrate, ferrihydrite, haemosiderin and ferritin as revealed by electron energy-loss spectroscopy. *Ultramicroscopy* 2010;**110**(8):1020-32.
28. Johnson JL, Cannon M, Watt RK, Frankel RB, Watt GD. Forming the phosphate layer in reconstituted horse spleen ferritin and the role of phosphate in promoting core surface redox reactions. *Biochemistry* 1999;**38**(20):6706-13.
29. Lopez-Castro JD, Delgado JJ, Perez-Omil JA, Galvez N, Cuesta R, Watt RK, et al. A new approach to the ferritin iron core growth: influence of the H/L ratio on the core shape. *Dalton Trans* 2012;**41**(4):1320-4.
30. Bejjani S, Pullakhandam R, Punjal R, Nair KM. Gastric digestion of pea ferritin and modulation of its iron bioavailability by ascorbic and phytic acids in caco-2 cells. *World J Gastroenterol* 2007;**13**(14): 2083-8.
31. Kalgaonkar S, Lonnerdal B. Receptor-mediated uptake of ferritin-bound iron by human intestinal Caco-2 cells. *J Nutr Biochem* 2009;**20**(4): 304-11.
32. Hoppler M, Schonbachler A, Meile L, Hurrell RF, Walczyk T. Ferritin–iron is released during boiling and in vitro gastric digestion. *J Nutr* 2008; **138**(5):878-84.
33. Kidane TZ, Sauble E, Linder MC. Release of iron from ferritin requires lysosomal activity. *Am J Physiol Cell Physiol* 2006;**291**(3):C445-55.
34. Masuda H, Ishimaru Y, Aung MS, Kobayashi T, Kakei Y, Takahashi M, et al. Iron biofortification in rice by the introduction of multiple genes involved in iron nutrition. *Sci Rep* 2012;**2**:543.
35. Murgia I, Arosio P, Tarantino D, Soave C. Biofortification for combating 'hidden hunger' for iron. *Trends Plant Sci* 2012;**17**(1):47-55.
36. Sperotto RA, Ricachenevsky FK, Waldow Vde A, Fett JP. Iron biofortification in rice: it's a long way to the top. *Plant Sci* 2012;**190**: 24-39.
37. Stein AJ, Meenakshi JV, Qaim M, Nestel P, Sachdev HP, Bhutta ZA. Potential impacts of iron biofortification in India. *Soc Sci Med* 2008;**66** (8):1797-808.
38. Powell J, Bruggraber S, Faria N, Pereira D, inventors. Ligand modified poly oxo-hydroxy metal ion materials, their uses and processes for their preparation. U.K. patent WO/2008/096130 2008 06.02.2008.
39. Cornell RM, Schwertmann U. Influence of organic-anions on the crystallization of ferrihydrite. *Clay Clay Miner* 1979;**27**(6):402-10.
40. Raja KB, Jafri SE, Dickson D, Acebron A, Cremonesi P, Fossati G, et al. Involvement of iron (ferric) reduction in the iron absorption mechanism of a trivalent iron-protein complex (iron protein succinylate). *Pharmacol Toxicol* 2000;**87**(3):108-15.
41. Reeves PG, Nielsen FH, Fahey Jr GC. AIN-93 purified diets for laboratory rodents: final report of the American Institute of Nutrition ad hoc writing committee on the reformulation of the AIN-76A rodent diet. *J Nutr* 1993;**123**(11):1939-51.
42. Hilty FM, Teleki A, Krumeich F, Buchel R, Hurrell RF, Pratsinis SE, et al. Development and optimization of iron- and zinc-containing nanostructured powders for nutritional applications. *Nanotechnology* 2009;**20**(47):475101.
43. Jambor JL, Dutrizac JE. Occurrence and constitution of natural and synthetic ferrihydrite, a widespread iron oxyhydroxide. *Chem Rev* 1998; **98**(7):2549-86.
44. Russell JD. Infrared spectroscopy of ferrihydrite—evidence for the presence of structural hydroxyl-groups. *Clay Miner* 1979;**14**(2): 109-14.
45. Cornell RL, Schwertmann U. *The iron oxides: structure, preparation, reactions, occurrences and uses*. 2nd ed. Weinham: Wiley-VCH; 2003.
46. Pan Y. *Electron microscopy study of mineral cores in ferritin and haemosiderin*. Leeds: University of Leeds; 2007.
47. Pan Y, Brown A, Brydson R, Warley A, Li A, Powell J. Electron beam damage studies of synthetic 6-line ferrihydrite and ferritin molecule cores within a human liver biopsy. *Micron* 2006;**37**(5):403-11.
48. Martell AE, Smith RM, Motekaitis RJ. *NIST critically selected stability constants of metal complexes database version 8.0*. National Institute of Standards and Technology: Gaithersburg; 2004.
49. Timberlake CF. Iron–tartrate complexes. *J Chem Soc* 1964:1229-40.
50. Galloway R, McGuire J. Determinants of compliance with iron supplementation: supplies, side effects, or psychology? *Soc Sci Med* 1994;**39**(3):381-90.
51. Hyder SM, Persson LA, Chowdhury AM, Ekstrom EC. Do side-effects reduce compliance to iron supplementation? A study of daily- and weekly-dose regimens in pregnancy. *J Health Popul Nutr* 2002;**20**(2): 175-9.
52. Lund EK, Wharf SG, Fairweather-Tait SJ, Johnson IT. Oral ferrous sulfate supplements increase the free radical-generating capacity of feces from healthy volunteers. *Am J Clin Nutr* 1999;**69**(2):250-5.
53. Wegmuller R, Zimmermann MB, Moretti D, Arnold M, Langhans W, Hurrell RF. Particle size reduction and encapsulation affect the bioavailability of ferric pyrophosphate in rats. *J Nutr* 2004;**134**(12): 3301-4.
54. Harvey RS, Reffitt DM, Doig LA, Meenan J, Ellis RD, Thompson RP, et al. Ferric trimaltol corrects iron deficiency anaemia in patients intolerant of iron. *Aliment Pharmacol Ther* 1998;**12**(9):845-8.
55. Michel FM, Barron V, Torrent J, Morales MP, Serna CJ, Boily JF, et al. Ordered ferrimagnetic form of ferrihydrite reveals links among structure, composition, and magnetism. *Proc Natl Acad Sci U S A* 2010;**107**(7): 2787-92.
56. Geisser P. Safety and efficacy of iron(III)-hydroxide polymaltose complex/a review of over 25 years experience. *Arzneimittelforschung* 2007;**57**(6A):439-52.
57. Van Wyck DB, Martens MG, Seid MH, Baker JB, Mangione A. Intravenous ferric carboxymaltose compared with oral iron in the treatment of postpartum anemia: a randomized controlled trial. *Obstet Gynecol* 2007;**110**(2 Pt 1):267-78.
58. Lane RS. Intravenous infusion of iron–dextran complex for iron-deficiency anaemia. *Lancet* 1964;**1**(7338):852-4.
59. Bisbe E, Garcia-Erce JA, Diez-Lobo AI, Munoz M. A multicentre comparative study on the efficacy of intravenous ferric carboxymaltose and iron sucrose for correcting preoperative anaemia in patients undergoing major elective surgery. *Br J Anaesth* 2011;**107** (3):477-8.
60. Lindgren S, Wikman O, Befrits R, Blom H, Eriksson A, Granno C, et al. Intravenous iron sucrose is superior to oral iron sulphate for correcting anaemia and restoring iron stores in IBD patients: a randomized, controlled, evaluator-blind, multicentre study. *Scand J Gastroenterol* 2009;**44**(7):838-45.
61. Eusterhues K, Wagner FE, Hausler W, Hanzlik M, Knicker H, Totsche KU, et al. Characterization of ferrihydrite-soil organic matter coprecipitates by X-ray diffraction and Mossbauer spectroscopy. *Environ Sci Technol* 2008; **42**(21):7891-7.
62. Mikutta C. X-ray absorption spectroscopy study on the effect of hydroxybenzoic acids on the formation and structure of ferrihydrite. *Geochim Cosmochim Ac* 2011;**75**(18):5122-39.

63. Latunde-Dada GO, Simpson RJ, McKie AT. Duodenal cytochrome B expression stimulates iron uptake by human intestinal epithelial cells. *J Nutr* 2008;**138**(6):991-5.
64. Raja KB, Simpson RJ, Peters TJ. Investigation of a role for reduction in ferric iron uptake by mouse duodenum. *Biochim Biophys Acta* 1992;**1135**(2):141-6.
65. Raja KB, Pountney D, Bomford A, Przemioslo R, Sherman D, Simpson RJ, et al. A duodenal mucosal abnormality in the reduction of Fe(III) in patients with genetic haemochromatosis. *Gut* 1996;**38**(5):765-9.
66. Wollenberg P, Rummel W. Dependence of intestinal iron absorption on the valency state of iron. *Naunyn Schmiedebergs Arch Pharmacol* 1987; **336**(5):578-82.
67. Pereira DI, Mergler BI, Faria N, Bruggraber SF, Aslam MF, Poots LK, et al. Caco-2 cell acquisition of dietary iron(III) invokes a nanoparticulate endocytic pathway. *PLoS One* 2013;**8**(11):e81250.
68. Chasteen ND, Harrison PM. Mineralization in ferritin: an efficient means of iron storage. *J Struct Biol* 1999;**126**(3):182-94.
69. Barron V, Torrent J, de Grave E. Hydromaghemite, an intermediate in the hydrothermal transformation of 2-line ferrihydrite into hematite. *Am Mineral* 2003;**88**(11–12):1679-88.
70. Deller DJ, Edwards RG, Dart G, Luke CG, Davis PS. Gastric iron binding substance (gastroferrin) in a family with haemochromatosis. *Australas Aann Med* 1969;**18**(1):36-42.
71. Rudzki Z, Baker RJ, Deller DJ. The iron-binding glycoprotein of human gastric juice. II. Nature of the interaction of the glycoprotein with iron. *Digestion* 1973;**8**(1):53-67.
72. San Martin CD, Garri C, Pizarro F, Walter T, Theil EC, Nunez MT. Caco-2 intestinal epithelial cells absorb soybean ferritin by mu(2) (AP2)-dependent endocytosis. *J Nutr* 2008;**138**(4):659-66.
73. Hilty FM, Arnold M, Hilbe M, Teleki A, Knijnenburg JT, Ehrensperger F, et al. Iron from nanocompounds containing iron and zinc is highly bioavailable in rats without tissue accumulation. *Nat Nanotechnol* 2010;**5** (5):374-80.